J. Water Environ. Nanotechnol., 10(3): 251-267 Summer 2025

ORIGINAL RESEARCH PAPER

Peroxi-Electrocoagulation removal of heavy metal particles by a stainless steel electrode coated with TiO_2 nanoparticles and an Iron electrode

Angham Sami Hamze[1], Majid Peyravi[1]*, Furat Yasir aljaberi[2]

[1] Department of Chemical Engineering, Babol Noshirvani University of Technology, Shariati Ave., Babol, Iran, Post Code:47148-71167
[2] Al-Muthanna University, Department of Chemical Engineering, Iraq

Received: 2025-01-29 Accepted: 2025-03-21 Published: 2025-08-01

ABSTRACT

This study explored cadmium removal from aqueous solutions using peroxi-electrocoagulation (PEC) with iron and TiO_2-coated stainless steel electrodes, varying geometry (non-perforated/perforated). FESEM, FTIR, and EDX characterized the TiO_2 coating. Response surface methodology (RSM) and Box-Behnken design (BBD) optimized electrocoagulation (EC), determining pH 6, 1.2 A current, and 62 minutes as optimal. Subsequently, PEC was conducted under these conditions (100 mg/L cadmium), examining electrode material and shape effects with/without H_2O_2. 80-minute experiments assessed pH/temperature variations. The iron electrode configuration achieved 97.1% (with H2O2) and 97.07% (without H_2O_2) cadmium removal. The iron anode/ TiO_2-coated stainless steel cathode achieved 95% (with H_2O_2) and 96.66% (without H_2O_2). Energy consumption for iron electrodes was 13.41 kWh/m³ (with H_2O_2) and 14.14 kWh/m³ (without H_2O_2), while the iron anode/ TiO_2-coated stainless steel cathode consumed 13.54 kWh/m³ (with H_2O_2) and 11.81 kWh/m³ (without H_2O_2). Kinetic analysis showed first-order kinetics for iron electrodes without H_2O_2, and both configurations with H_2O_2. Thermodynamic analysis indicated an endothermic, non-spontaneous, and chaotic process. Moreover, FTIR examined the electrode geometry. Results showed the iron electrode configuration with H_2O_2 provided the most effective removal with lower energy consumption.

Keywords: *PEC electrodes, nano-coated electrode, Electrocoagulation, TiO2 Nanoparticle, Water pollution.*

How to cite this article
Sami Hamze A., Peyravi M., Yasir aljaberi F. Peroxi-Electrocoagulation removal of heavy metal particles by a stainless steel electrode coated with TiO_2 nanoparticles and an Iron electrode. J. Water Environ. Nanotechnol., 2025; 10(3): 251-267.
DOI: 10.22090/jwent.2025.03.002

INTRODUCTION

Intensifying industrial activities are placing increasing pressure on global freshwater resources [1]. The discharge of a diverse range of chemicals resulting from these activities poses a serious threat to the ecological balance that sustains life on Earth [2]. Even trace amounts of pollutants in water pose a serious risk to humans, animals, and plants, causing a wide range of diseases and mortality. The lack of proper wastewater treatment systems allows harmful and non-biodegradable chemicals to accumulate in water sources [3]. These persistent pollutants, including pesticides, hydrocarbons, plasticizers, and synthetic dyes, pose a serious threat to aquatic and terrestrial ecosystems [4]. In addition to organic pollutants, inorganic pollutants such as heavy metals, including arsenic, cadmium, mercury, and lead, pose significant risks to aquatic ecosystems. Various wastewater treatment techniques, including membrane filtration, adsorption, ion exchange, extraction, and precipitation, have been

* Corresponding Author Email: *majidpeyravi@nit.ac.ir*
majidpeyravi@gmail.com

This work is licensed under the Creative Commons Attribution 4.0 International License.
To view a copy of this license, visit http://creativecommons.org/licenses/by/4.0/.

investigated for the removal of contaminants from water resources [5-7]. However, each of these methods presents inherent limitations that restrict their widespread application in decolorization processes [8]. Consequently, there is a growing trend among researchers towards the adoption of chemical and electrochemical techniques, owing to their promising results. Among these, advanced oxidation processes (AOPs) stand out, which rely on the reactivity of hydroxyl radicals (•OH) generated from water or hydrogen peroxide (H_2O_2) [7, 9]. To enhance the formation of •OH radicals, AOPs are frequently integrated or modified with electrochemical or photochemical processes [10].

Electrochemical advanced oxidation processes (EAOPs) provide a compelling pathway for environmentally responsible wastewater remediation, harnessing electrons for the in-situ generation of potent oxidants [11, 12]. Among the EAOP family, the electro-Fenton (EF) process stands out due to its operational advantages. Unlike direct electrochemical oxidation (EO), which generates •OH radicals at the anode surface (Eq. 1), EF produces •OH within the bulk solution [13]. This is accomplished through the controlled two-electron reduction of oxygen to H_2O_2 at a carbonaceous cathode (Eq. 2) [14]. This in-situ H_2O_2 generation eliminates the need for external oxidant storage and the handling of the process. Moreover, the EF system efficiently regenerates the Fe^{2+} catalyst through the electrochemical reduction of Fe^{3+} (Eq. 3), contributing to its sustained effectiveness [14]. Consequently, EF presents a promising avenue for efficient and sustainable contaminant degradation.

$$M + H_2O_2 \rightarrow M(\bullet OH) + H^+ + e^- \quad (1)$$

$$O_2(g) + 2H^+ + 2e^- \rightarrow H_2O_2 \quad (2)$$

$$Fe^{3+} + e^- \rightarrow Fe^{2+} \quad (3)$$

While the EF process is recognized for its rapid oxidation kinetics, it suffers from operational challenges, including the requirement for acidic pH, the need for post-treatment neutralization, and significant sludge generation due to high iron consumption. Among EAOPs, peroxi-electrocoagulation (PEC) has gained considerable attention for its potential in wastewater treatment. PEC builds upon the well-established Fenton reaction, where •OH radicals are generated via the interaction of Fe^{2+} with H_2O_2, as shown in Eq. 4-7 [14, 15].

$$Fe^{2+} + H_2O_2 \rightarrow Fe^{3+} + \bullet OH + OH^- \quad (4)$$

$$RH + \bullet OH \rightarrow R\bullet + H_2O \quad (5)$$

$$R\bullet + Fe^{3+} \rightarrow Fe^{2+} + R^+ \quad (6)$$

$$Fe^{2+} + \bullet OH \rightarrow OH^- + Fe^{3+} \quad (7)$$

However, PEC distinguishes itself by electrochemically generating Fe^{2+} using iron electrodes and an applied current, rather than relying on direct Fe^{2+} addition [16]. The resulting •OH radicals effectively degrade organic pollutants through radical-mediated pathways, leading to their mineralization. PEC addresses these limitations by facilitating the electrochemical regeneration of Fe^{2+} at the cathode, thereby reducing sludge production and minimizing the need for external iron supplementation. This in-situ regeneration mechanism makes PEC a more sustainable and operationally efficient alternative to the conventional Fenton process [17].

Researchers have explored various wastewater treatment techniques for removing heavy metals from water. For example, Xu et al. demonstrated heavy metal removal efficiencies exceeding 97% using electrocoagulation, while Xia et al. achieved over 99% cadmium removal from groundwater with Fenton-like processes [18, 19]. Despite these advances, the application of the PEC process for heavy metal removal remains limited. Furthermore, a comparative study of PEC's efficiency with and without hydrogen peroxide (H_2O_2) is necessary to evaluate the benefits of external H_2O_2 addition, which increases operational costs. This study investigates cadmium removal from aqueous solutions using PEC. To optimize treatment, response surface methodology (RSM), specifically Box-Behnken design (BBD), was employed to determine optimal operating parameters, addressing the limitations of traditional single-variable optimization [20, 21]. Initially, BBD was used to establish optimal (EC) conditions with iron electrodes. Subsequently, the study evaluated the influence of electrode shape (perforated vs. unperforated) and material (iron vs. TiO_2-coated stainless steel) on cadmium removal under the optimal conditions established during the EC process. Additionally,

CC BY

critical factors such as pH, temperature, electrode consumption, thermodynamic parameters, and energy consumption were examined throughout the reaction.

EXPERIMENTAL

Chemicals

To prepare the synthetic wastewater, Cd $(NO_3)_2.4H_2O$ (95%) was dissolved in the supporting electrolyte at the specified concentrations, and a specified concentration of H_2O_2 with 0.5 g/L of NaCl in the solution was employed as the supporting electrolyte. The pH of the solution was adjusted to the desired range using 0.1 N hydrochloric acid (HCl) and 0.1 N sodium hydroxide (NaOH). Electrodes were cleaned with dilute hydrochloric acid, followed by distilled water to remove any accumulated deposits. All chemical reagents used in this study were acquired from commercial suppliers. Specifically, nitric acid (HNO_3, 65 wt.%), aqueous ammonia (25 wt.%), titanium (IV) butoxide (TBOT), isopropyl alcohol, acetone, and ethanol were obtained from Merck and Sigma-Aldrich.

Electrodes Design and Arrangement

A PEC batch reactor with two cylindrical electrodes of different diameters and materials was used for heavy metal removal from water. The active area of the cathode electrodes (CE-1 and CE-2) was 131 cm^2, while the active area of the anode electrode (AE) was 252 cm^2. Fig. 1 and table. 1 Shows the anode and cathode electrodes design and dimensions.

In the experimental setup, a concentric electrode configuration was used with a perforated cathode positioned within an unperforated anode. A fixed inter-electrode distance of 2 cm was maintained throughout the experiments. To ensure optimal performance, the electrodes were cleaned regularly to remove accumulated oxide layers and dried before subsequent use.

Electrode coating process

Electrode fabrication involved a multi-step chemical treatment of stainless-steel substrates. Initial surface decontamination was achieved through sequential sonication in acetone, ethanol, and deionized water. Subsequent oxide removal

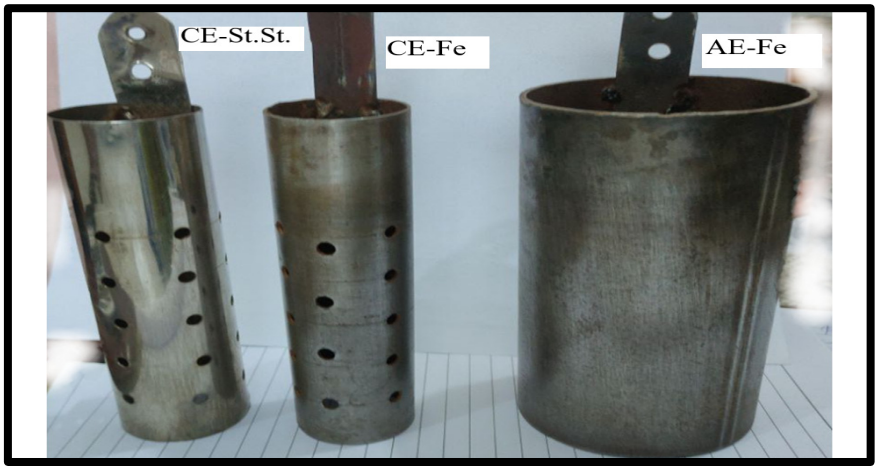

Fig. 1. The design and configurations of electrodes

Table 1. Cylindrical Electrodes dimensions.

Electrode	AE-Fe	CE-Fe	CE-St. St.
Anode/ Cathode	anode	cathode	cathode
cylinder/ Perforated	nonperforated	perforated	perforated
Dimensions (cm)	15×7.3	15×3.8	15×3.8
Electrode Thickness (cm)	1.5	1.5	0.5
Distance between electrodes (cm)	2	2	2
Wet height (cm)	11	11	11
Active area (cm^2)	252	131	131

(cc) BY

was performed via immersion in a 3 M HNO_3 bath. TBOT precursor solution (0.075 M) was then applied to the cleaned substrates through a triple dip-coating process, with intermediate drying at 60 °C after each application. TiO_2 formation was induced by a post-coating hydrothermal anneal at 600 °C within a tube furnace. Finally, the resulting TiO2-coated electrodes were thoroughly rinsed with deionized water, followed by ethanol [18].

Characteristics of prepared electrodes

A comprehensive material characterization of the stainless-steel electrodes was performed using several analytical methods. Surface morphology was examined via field emission scanning electron microscopy (FESEM, Mira 3-XMU). X-ray diffraction (XRD) analysis was conducted to determine the crystalline structure of the TiO_2 coatings. Fourier-transform infrared spectroscopy (FTIR, TENSOR 27, Germany) was used to probe the chemical bonding and molecular structure of the coated electrodes.

Experimental design

Response surface methodology (RSM) was utilized as a statistical tool aiming to optimize the response surface affected by several parameters. RSM also provided a relationship between the independent input factors and the response variable [22, 23]. In this research, the optimization of experiments for the removal of Cadmium wastewater by electrocoagulation was carried out using a Box-Behnken design. To investigate the effect of the operating variable on the Cadmium removal efficiency, three major factors were considered: reaction time (min) (X_1), applied current (A) (X_2), and pH (X_3) as illustrated in Table 2.

The experimental data (Table 3) were analyzed using the response surface regression (RSREG) procedure to fit a second-order polynomial model [24]:

$$Y = \beta_0 + \sum_{i=1}^{k}\beta_i X_i + \sum_{i=1}^{k}\beta_{ii} X_i^2 + \sum_{i=1}^{k}\sum_{j=1}^{k}\beta_{ij} X_i X_j + \varepsilon \qquad (8)$$

Where Y represents the response (Cadmium removal efficiencies, %), and $\beta_0, \beta_i\,(i=1,2,3)$, and $\beta_{i,j}\,(i=1,2,3; j=1,2,3)$ are the model coefficients, with X_i and X_j As the coded independent variables. Optimum conditions from the BBD model were chosen to establish a baseline for comparing the performance of two distinct electrode configurations. Both configurations, with and without the addition of H_2O_2, were evaluated, and their specifications are shown in the Table. 3.

PEC experiments

In this study, PEC experiments were conducted in a cylinder glass cell of 1301 ml volume at room temperature as depicted in Fig. 2. The solution contained within the PEC reactor was subjected to continuous stirring at a consistent rotational speed using a magnetic stirrer and the electrodes were connected to a DC power supply (DC power supply type SYADGONG, China) with an electronic pH meter was utilized to measure the pH value over time for each experiment. The Cd concentration of 100 mg/l was used for each experiment, and at the end of each one, the quantities of Cd determined through analysis by using an atomic absorption spectrometer (Shimadzu, Japan, model AA-7000F), and the Cd removal efficiency (Y_{cd}) was estimated using Eq. 9 [25]:

Table 2. Actual and coded values of the variables of the experimental design for the electrocoagulation process

Factors	variables	Coded levels of variables		
		-1	0	+1
X_1	Reaction time (min)	10	45	80
X_2	Applied current (A)	0.8	1.2	1.6
X_3	PH	2	6	10

Table 3. Different Types of electrode configurations and materials in the presence and absence of H_2O_2

Types	Configuration kinds	Anode electrode	Cathode electrode	H_2O_2
Type 1	one tube (anode) iron (nonperforated)	Outer	Inner	✓
	one tube (cathode) iron (perforated)	Outer	Inner	×
Type 2	one tube (anode) iron (nonperforated)	Outer	Inner	✓
	one tube (cathode) stainless steel coated with TiO_2 (perforated)	Outer	Inner	×

$$Y_i = \frac{C_i - C_t}{C_i} \times 100 \quad (9)$$

Where the concentrations of Cd at time (0) and (t) were denoted as C_0 and C_t, respectively. Moreover, Eq. 10 has been used for describing the energy consumption in either (kWh/m^3) or (kWh/kg):

$$ENC = \frac{VIT}{V_R} \quad (10)$$

Where V is the voltage of the cell in volts, I is current intensity in amperes, T is the time of the reaction in hours, and V_R is the volume of the wastewater sample in cubic meters. Besides, the actual electrode consumption measured through the change in weight for the electrode between the starting and ending points for each experiment, which that measured under these conditions by using Eq. 11 [30, 31]:

$$TC = \frac{ItM}{ZF} \quad (11)$$

Where I is current intensity in ampere, t is time of the reaction in seconds, M is electrode molecular weight in (g/mol), Z is number of electrons (2 for iron), F is Faraday's constant 96,485.34 Columb/mol.

Equations 12 and 13 describe the thermodynamic parameters, including the standard enthalpy change (ΔH°), standard Gibbs free energy change (ΔG°), and standard entropy change (ΔS°), which were evaluated as a function of temperature during electrolysis, while maintaining other variables constant. Furthermore, the slope of the Van't Hoff plot derived from Eq. 14 provides an estimate of ΔH° [28].

$$\Delta G° = \Delta H° - T\Delta S° \quad (12)$$

$$\Delta G° = -RT\ln k_d \quad (13)$$

In the above equations, R is the standard gas constant (8.314J/mol. K); T is absolute temperature (K); K_d is the equilibrium constant, and it can be calculated by using the equations (14), (15), and (16) [34]:

$$\log k_d = -\frac{\Delta H}{2.303RT} + \text{constant} \quad (14)$$

$$k_d = \frac{q_e}{C_e} \times \frac{m}{V} \quad (15)$$

$$q_e = \frac{[C_i - C_e] \times V}{m} \quad (16)$$

q_e is the adsorbate amount (mg/g); C_i, C_e is the initial and equilibrium concentration of the adsorb (mg/L); m is the mass of the adsorbent (g); V is the volume of the solution (L).

To study the reaction rate in the electrochemical reactor and to evaluate the reaction rate constants, equation (17) was used with the current electrode arrangement [26].

$$\frac{dC_t}{dC_t} = -KC_t^n \quad (17)$$

C_t: concentration of Cd metal at any time, K: reaction rate constant, t: time of the reaction.

RESULTS AND DISCUSSION

Electrode characterization

Microstructural and compositional analyses were performed on the TiO_2 nanoparticle-modified stainless-steel electrode. FESEM images (Fig. 3a-c, varying magnifications) revealed the successful deposition of nanosized, spirally shaped TiO_2 particles onto the substrate. XRD analysis (Fig. 3d) identified diffraction peaks at 43.7°, 50.9°, and 75.0°, consistent with the underlying stainless-steel substrate [27]. The relatively low intensity of these peaks may be attributed to the presence of the dense TiO_2 nanoparticle layer. Notably, the XRD pattern also confirmed the anatase crystalline phase of the TiO_2 nanoparticles, with characteristic peaks observed at 25.3°, 37.8°, 48.0°, 54.9°, and 62.7°, corresponding to the (101), (112), (200), (211), and (204) crystallographic planes, respectively (JCPDS 00-021-1272) [28].

ATR-FTIR (Fig. 3e) further characterized the chemical composition of the modified electrode. A broad absorption band in the 3400–3500 cm^{-1} region indicated the presence of surface hydroxyl groups and physically adsorbed water [29]. The TiO_2 network formation was confirmed by the presence of a characteristic peak at 880 cm^{-1}, attributed to O–Ti–O bond stretching vibrations [30]. A peak at 1604 cm^{-1} suggested the chemisorption of water molecules via H–O–H bending vibrations [31], while a peak at 1438 cm^{-1} further corroborated the presence of Ti–O bonds [32].

Response analysis by Box–Behnken design (BBD)

The design matrix for the variables: reaction

CC BY

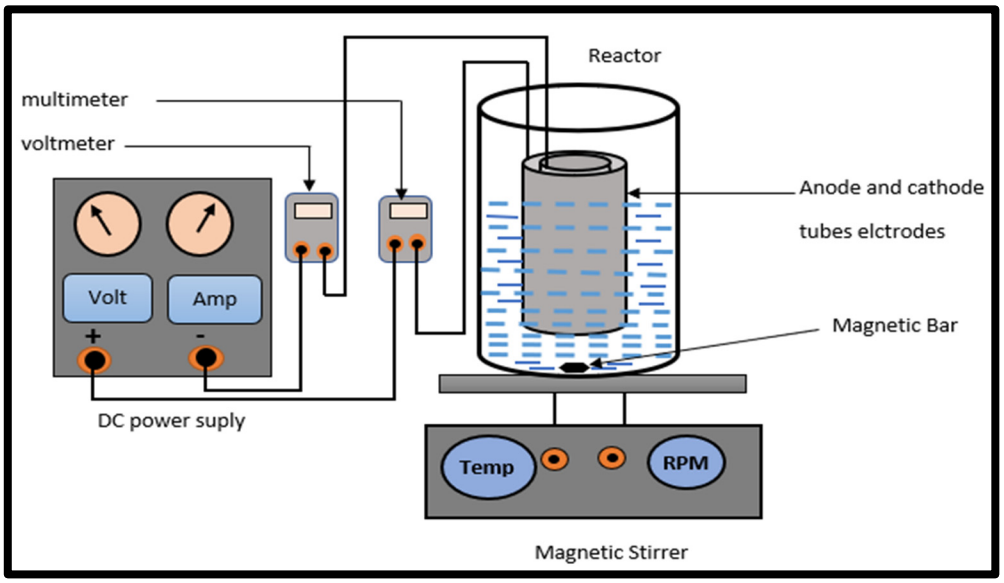

Fig. 2. Schematic of the electrocoagulation apparatuses

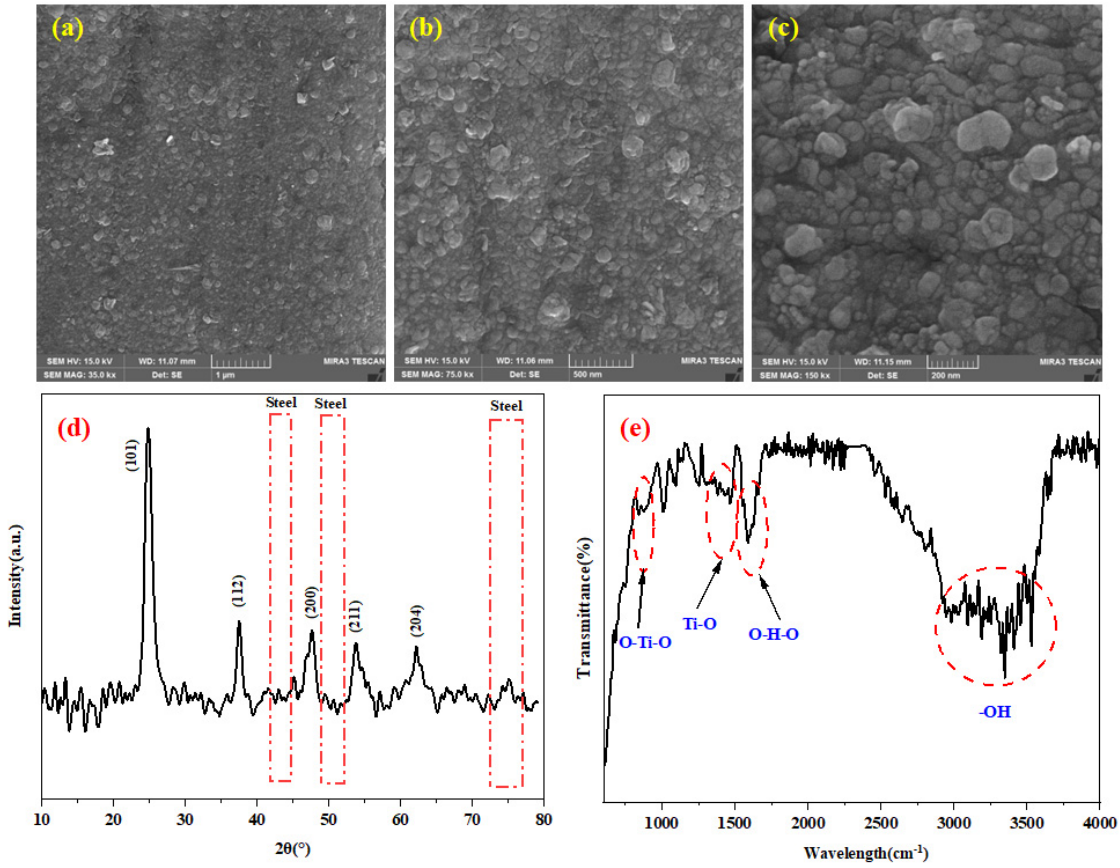

Fig. 3. FESEM images of coated electrode with TiO_2 nanoparticles with different magnification (a-c), XRD pattern (d), and ATR-FTIR absorbance spectra (e) of the coated electrode.

Table 4. Experimental design matrix and responses based on the experiment runs and predicted values on Cd removal (%)

Run	Independent variables			Response	
	X_1 (min)	X_2 (A)	X_3	Experimental	Predicted
	Reaction time	Applied current	PH	Cadmium removal	Cadmium removal
1	80 (+1)	1.2 (0)	2 (-1)	55.55	56.23
2	10 (-1)	0.8 (-1)	6 (0)	49.79	50.48
3	45 (0)	1.2 (0)	6 (0)	91.27	91.98
4	45 (0)	0.8 (-1)	2 (-1)	49.82	49.06
5	80 (+1)	1.2 (0)	10 (+1)	72.51	72.45
6	45 (0)	1.2 (0)	6 (0)	91.72	91.90
7	80 (+1)	0.8 (-1)	6 (0)	69.96	70.03
8	45 (0)	1.2 (0)	6 (0)	92.39	91.90
9	80 (+1)	1.6 (+1)	6 (0)	95.41	94.71
10	45 (0)	1.2 (0)	6 (0)	92.51	91.90
11	45 (0)	0.8 (-1)	10 (+1)	52.85	52.83
12	10 (-1)	1.6 (+1)	2 (-1)	56.43	56.36
13	45 (0)	1.6 (+1)	2 (-1)	59.31	59.38
14	10 (-1)	1.2 (0)	2 (-1)	34.67	34.72
15	45 (0)	1.2 (0)	6 (0)	91.62	91.90
16	10 (-1)	1.2 (0)	10 (+1)	36.73	36.05
17	45 (0)	1.6 (+1)	10 (+1)	72.36	73.12

Table 5. Analysis of variance (ANOVA) and quadratic model fit for Cd removal (%)

Source	SS	df	MS	F-value	p-value	
Model	6988.40	9	776.49	1299.46	< 0.0001	Significant
X_1	1676.78	1	1676.78	2806.11	< 0.0001	
X_2	466.65	1	466.65	780.94	< 0.0001	
X_3	154.00	1	154.00	257.72	< 0.0001	
X_1X_2	88.36	1	88.36	147.87	< 0.0001	
X_1X_3	55.50	1	55.50	92.88	< 0.0001	
X_2X_3	25.10	1	25.10	42.01	< 0.0003	
X_1^2	1127.43	1	1127.43	1886.76	< 0.0001	
X_1^2	245.99	1	245.99	411.67	< 0.0001	
X_1^2	2775.28	1	2775.28	4644.45	< 0.0001	
Residual	4.18	7	0.5975			
Lack of Fit	3.06	3	1.02	3.65	0.1217	Not Significant
Pure Error	1.12	4	0.28			
Cor Total	6992.59	16				

$R^2 = 0.9994$; $R^2\ adj = 0.9986$; $R^2 = 0.9927$; df: degree of freedom; SS: Sum of Square; MS: Mean Square

time (min) (X_1), applied current (A) (X_2), and pH (X_3) in both uncoded and coded units determined by the BBD is presented in Table 4. The predicted response values for the percentage of Cd removal were derived using quadratic model fitting methods. The response functions for Cd removal, along with their determined coefficients, are presented in the Equation. (18).

$$Y = 91.9 + 14.48X_1 + 7.64X_2 + 4.39X_3 + 4.70X_1X_2 + 3.73X_1X_3 + 2.51X_2X_3 - 16.36X_1^2 - 7.64X_2^2 - 25.67X_3^2 \quad (18)$$

Analysis of variance (ANOVA) was performed for response, and the results were presented in Table 5, confirming that the model's predictability is at a 95% confidence level. The predicted values from the response function closely matched the data from the experiments, with R^2 values of 99.9% for Y. A comparison of the predicted values was calculated using Eq. 18, indicating that both the predicted and observed values were precise, as depicted in Figure 4. The quadratic regression model is highly significant, as demonstrated by Fisher's F-test, which resulted in a very low probability value (Prob > F = 0.0001). Given that the p-values for all coefficients were less than 0.05, indicating that all of them were statistically significant. The fit statistics were presented by R^2 value (0.9994) and the predicted R^2 value (0.9927),

CC BY

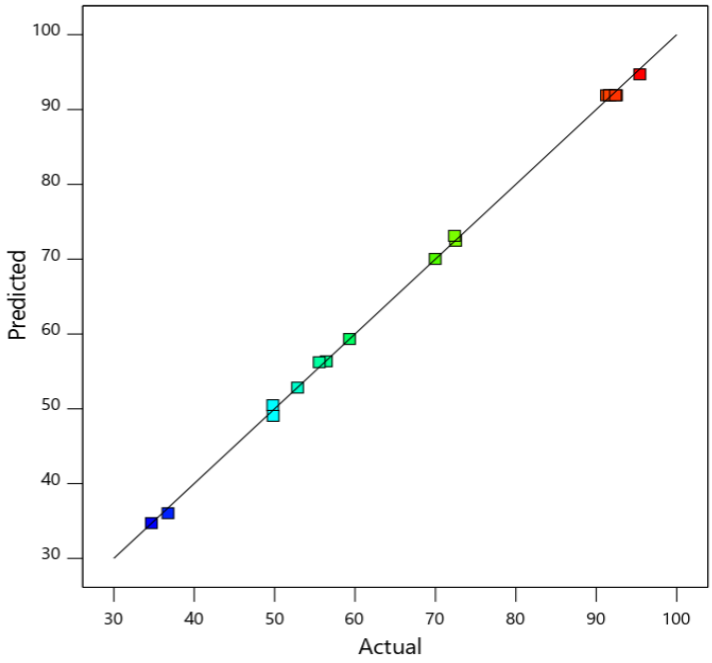

Figure 4. Regression plot of the predicted versus actual values

demonstrating a reasonable agreement with the adjusted R^2 value (0.9986) for Cadmium removal, as the differences between these values are less than 0.2 [33]. Meanwhile, the value of C.V.% (Coefficient of Variation) is 1.23% for the percentage of Cd removal, implying that the outcomes obtained are accurate.

Impact of different variables on Cadmium removal efficiency and interaction effects of parameters

The two-dimensional contour plots in Figure 5 show the interactions of the operating parameters for the Cadmium removal. As depicted in Figure 5(a) and (b), significant Cadmium removal efficiency was achieved along with the increase in the reaction time, especially as the electrolysis time extended from 10 to 60 minutes, Cadmium removal reached over 95% efficiency whilst maintaining the applied current and pH at their mid-level values. Furthermore, it can be seen from Figure 2(b and c) that the pH considerably influenced the Cadmium removal, since a greater amount of metal was removed with the pH decline from 10 to 6. The highest removal was achieved when the pH ranged roughly between 5.5 and 6.5, although further decreasing the pH to 2 at an unchanged 45 minutes of reaction time lowered Cadmium removal. According to Figure 2(a and c), increasing current had a positive impact on the removal efficiency since a slight growth in the removal rate was observed when a higher current was applied.

Optimization of the model

The software's numerical optimization method was chosen to detect the specific point that maximizes the desirability function. The optimum conditions were determined by setting the importance, which could affect the characteristics of the objective [34]. To determine the optimal process parameters for achieving the highest Cd removal efficiencies, the desirability function methodology was employed in this work, and the results are shown in the Table. 6.

Removal Efficiency

The optimal conditions for the EC process, as determined by BBD, were pH 6, an applied current of 1.2 A, and a reaction time of 60 minutes. To further examine the effects of reaction time, an extended duration of 80 minutes was also evaluated, specifically to observe changes in removal efficiency, pH, and solution temperature. The first type [i.e., the anode electrode from an iron cylindrical nonperforated, the cathode electrode from an iron cylindrical perforated] was used with two cases: in H_2O_2 presence case and its absence case. It was

CC BY

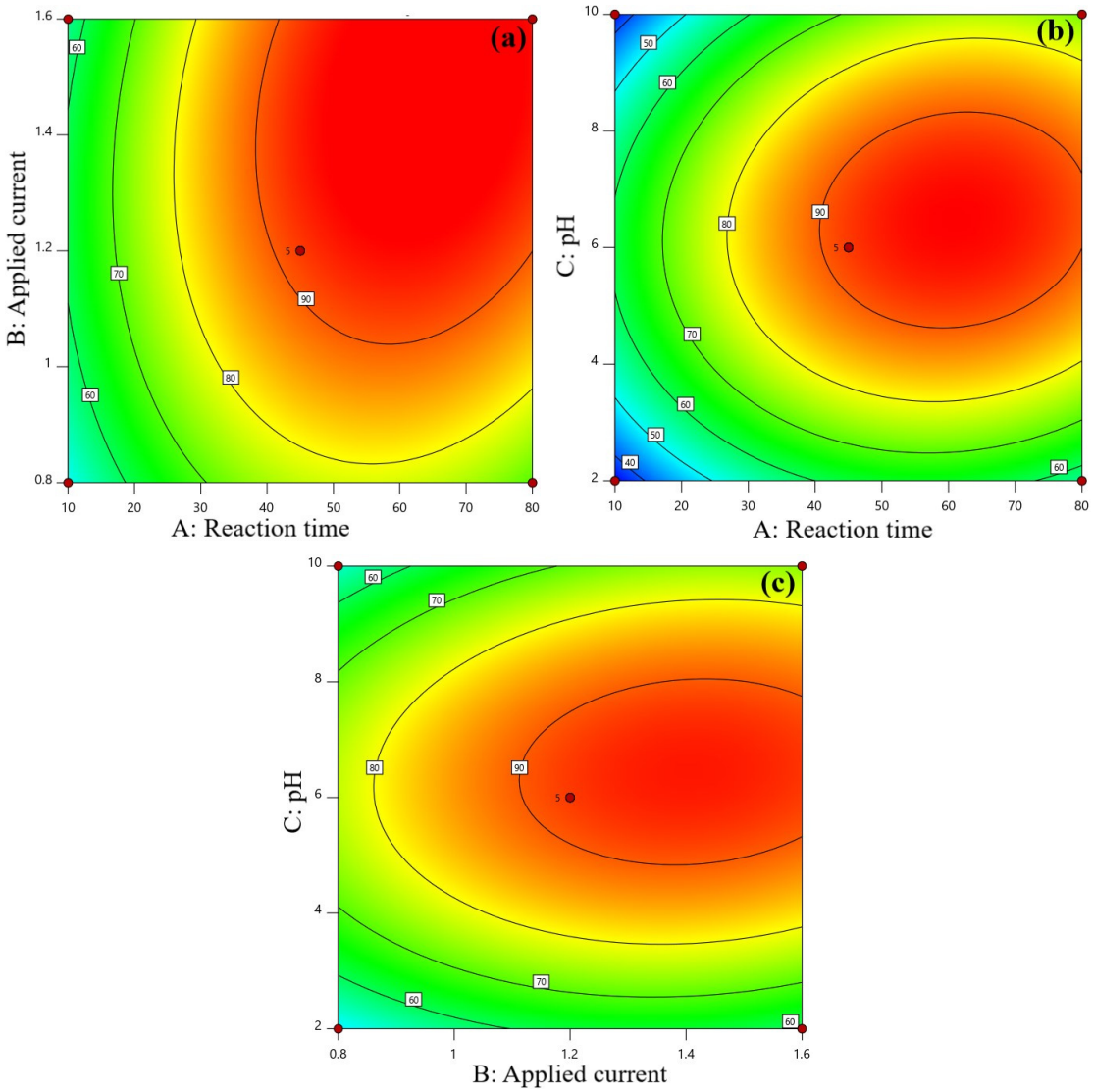

Fig. 5. The two-dimensional contour plots show the interactions of the operating parameters for the Cd removal (%)

Table 6. Optimum conditions for the electrocoagulation process for the iron electrode

Condition	variables			Response	Desirability
	Reaction time (min)	Applied current (A)	pH	Cadmium removal efficiency (%)	
Optimum	62.11	1.28	5.94	96.77	1.000

found that the efficiency of the Cd removal at the optimum condition in the presence of H_2O_2 was greater than when it was absent. Two primary factors contributed to this observation. Firstly, the significant dissolution of the anode electrode led to the formation of a substantial amount of adsorbent material. Secondly, the constant release of gas bubbles from all sides of the cathode electrode, essential for the adsorption process [35], and the abundant supply of hydroxyl ions from the active region surrounding the cathode further facilitated adsorption. However, equilibrium was reached at different times for the two scenarios: 10 minutes in the presence of H_2O_2 and 60 minutes

(cc) BY

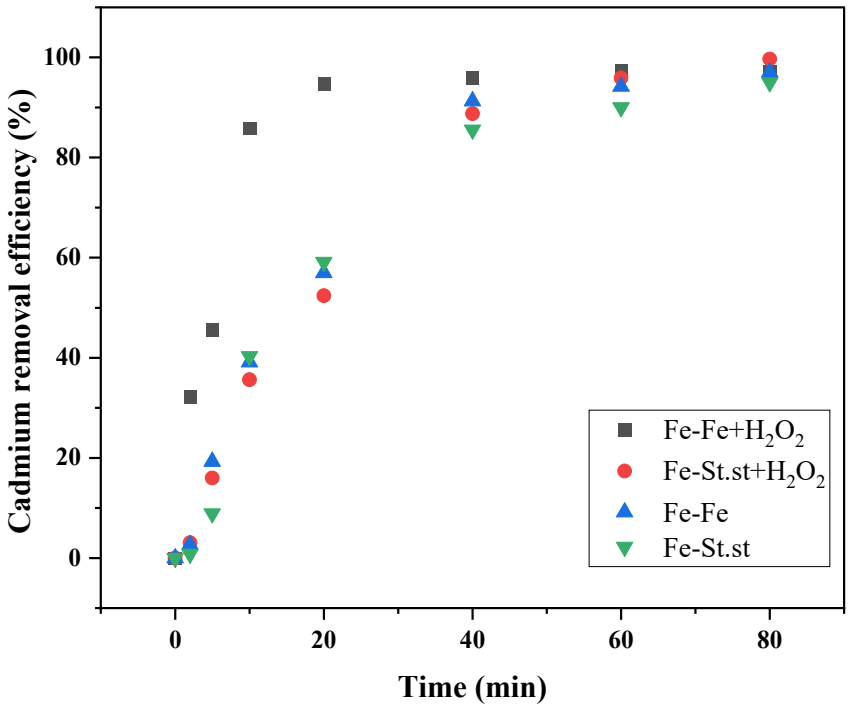

Fig. 6. The impact of electrode arrangement on the effectiveness of Cd removal (at optimum condition, pH=6, applied current=1.2 A, and reaction time=80 min)

Table 7. The impact of electrode arrangement on the effectiveness of Cd removal

Types	Configuration kinds	H_2O_2	after 10 min	after 60 min	after 80 min
			Removal efficiency (%)		
Type 1	one tube (anode) iron (nonperforated)	✓	85.76	97.3	97.1
	one tube (cathode) iron (perforated)	×	91.29	94.19	97.07
Type 2	one tube (anode) iron (nonperforated)	✓	88.78	95.92	96.66
	one tube (cathode) stainless steel coated with TiO_2 (perforated)	×	85.56	90	95

in its absence, as predicted by the optimization model. A second electrode configuration was tested, comprising an iron cylindrical non-perforated anode and a stainless steel coated with TiO_2 cylindrical perforated cathode. Two cases were investigated: with and without the presence of H_2O_2. Results indicated that the efficiency of Cd removal was higher in the presence of H_2O_2, although equilibrium was reached at the same time (60 minutes) in both cases. Table. 7 and 6 exhibit the four experiment results for time up to 80 min to explore the behavior of the new designs of all electrodes.

Changes in Temperature

At first, the temperature was around 25 °C in all the experiments, but it gradually increased throughout the electrolysis process due to the continuous passage of electrical current across the electrodes, which mobilized various ions that released heat as they made their way through the electrodes into the center of the polluted solution [36, 37]. Upon the completion of the treatment time, the final temperature was between 28°C and 30 °C in primary tests that were used and as depicted in Fig. 7.

Energy Consumption

A critical factor in the successful application of electrocoagulation for wastewater remediation is energy efficiency. Table. 8 and Fig. 8 reveal that the energy consumption of the first configuration

CC BY

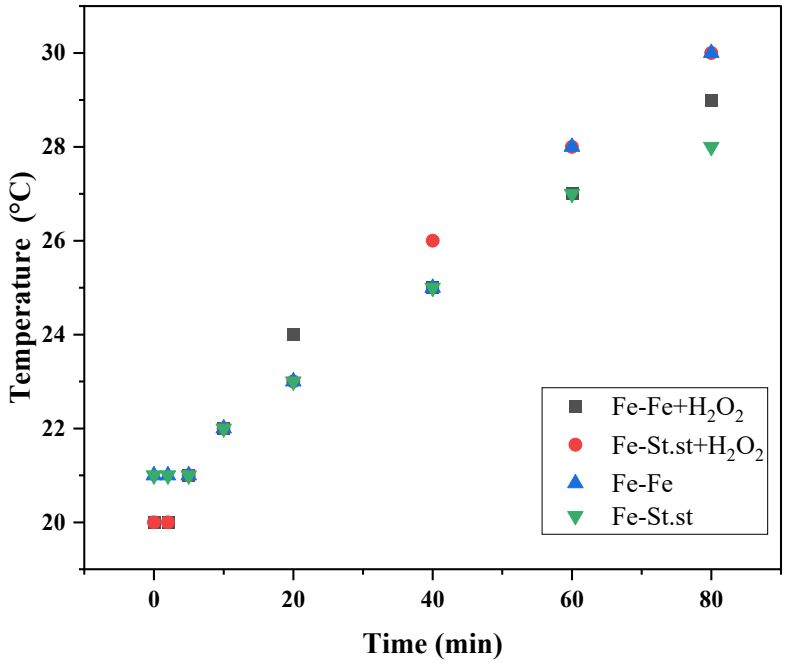

Fig. 7. The Effect of electrode configuration on the change of the interior temperature (at optimum condition, pH=6, applied current=1.2 A, and reaction time=80 min)

Table. 8. Electrode configuration's impact on power consumption

Types	Configuration kinds	H_2O_2	Energy consumption value (kWh/m^3)
Type 1	one tube (anode) iron (nonperforated)	✓	13.41
	one tube (cathode) iron (perforated)	×	14.14
Type 2	one tube (anode) iron (nonperforated)	✓	13.53
	one tube (cathode) stainless steel coated with TiO_2 (perforated)	×	11.81

(iron electrodes) was slightly higher in the absence of H_2O_2 compared to its presence, whereas the second configuration (iron and stainless-steel electrodes coated with TiO_2) exhibited higher energy consumption in the presence of H_2O_2. This discrepancy can be attributed to the increased over-potential ohmic drop between electrode pairs. The continuous release of energy-intensive ferrous ions from anode oxidation, exacerbated by the lack of a protective layer on the anode electrode, contributes to this elevated over-potential ohmic drop [38].

Electrodes Consumption

In each design, part of the weight of the electrodes had to be sacrificed to complete the electrocoagulation process. When compared between the two types, the first type, which used iron as anode and cathode, consumed less than the second type in both cases H_2O_2 presence and absence it. The reason may be that the sharing of the cathode in the reaction is consumed. Also, the first type, when used with the H_2O_2 presence, consumes more than when used in its absence it because the removal and efficiency of the reaction increases because the H_2O_2 presence. However, the second type has the same consumer from anode when used with or without H_2O_2 presence because it has the same range of removal. As shown in the Table. 9, the theoretical electrode consumption measured by Eq. 10 is higher than the theoretical value (Fig. 9).

A Streamlined Kinetics Method

Kinetic modeling was presented for the best configuration first type with H_2O_2 as a second-order reaction because more efficient at the highest regression coefficient, while the configuration of first type with the absence of H_2O_2 and second type with the presence absence H_2O_2 are first-order reactions, which are less efficient than a second-

(cc) BY

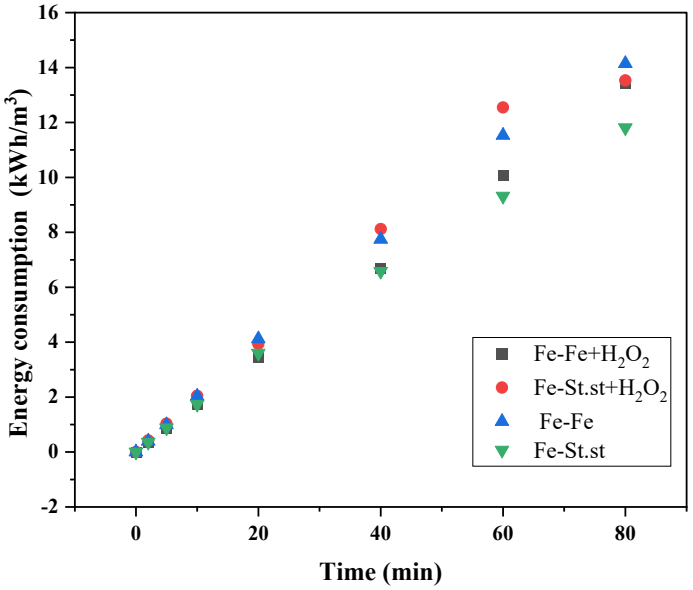

Fig. 8. Electrode configuration's impact on energy consumption (at optimum condition, pH=6, applied current=1.2 A, and reaction time=80 min)

Table. 9. The impact of electrode arrangement on the actual consumption of electrodes and the theoretical consumption of electrodes

Types	Configuration kinds	H_2O_2	Actual electrode consumption value (g/l)
Type 1	one tube (anode) iron (nonperforated)	✓	1.95
	one tube (cathode) iron (perforated)	×	1.92
Type 2	one tube (anode) iron (nonperforated)	✓	2.09
	one tube (cathode) stainless steel coated with TiO_2 (perforated)	×	2.09

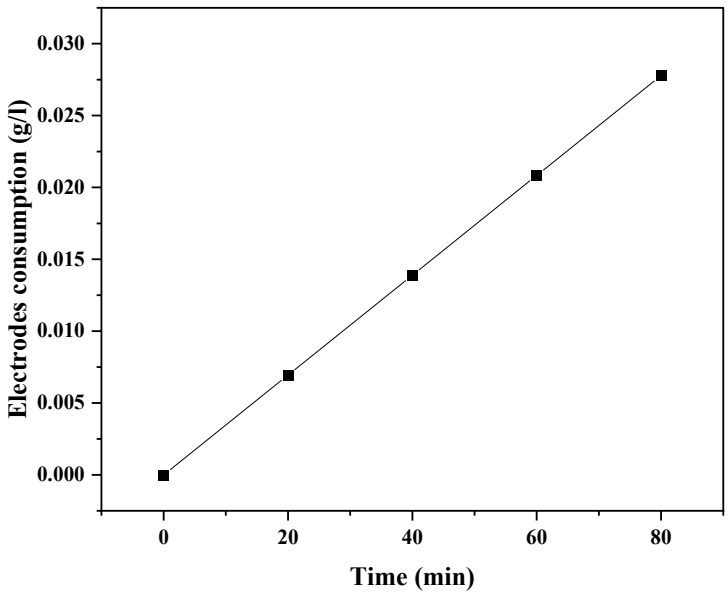

Fig. 9. The impact of electrode arrangement on the theoretical consumption of electrodes (at optimum condition, pH=6, applied current=1.2 A, and reaction time=80 min)

Table 10. The kinetic rate equations for different configurations

Types	Configuration kinds	H_2O_2	order	Simulated Equation	k unit $(mol/m^3)^{1-n}$	R^2
Type 1	one tube (anode) iron (nonperforated)	✓	2	$\frac{1}{C_t} = 0.0048\ t + 0.0371$	0.0048	0.91
	one tube (cathode) iron (perforated)	×	1	$-ln\frac{C_t}{C_i} = 0.0467$ t + 0.0325	0.0467	0.97
Type 2	one tube (anode) iron (nonperforated)	✓	1	$-ln\frac{C_t}{C_i} = 0.0666$ t - 0.2506	0.0666	0.96
	one tube (cathode) stainless steel coated with TiO_2 (perforated)	×	1	$-ln\frac{C_t}{C_i} = 0.0387$ t + 0.0438	0.0387	0.98

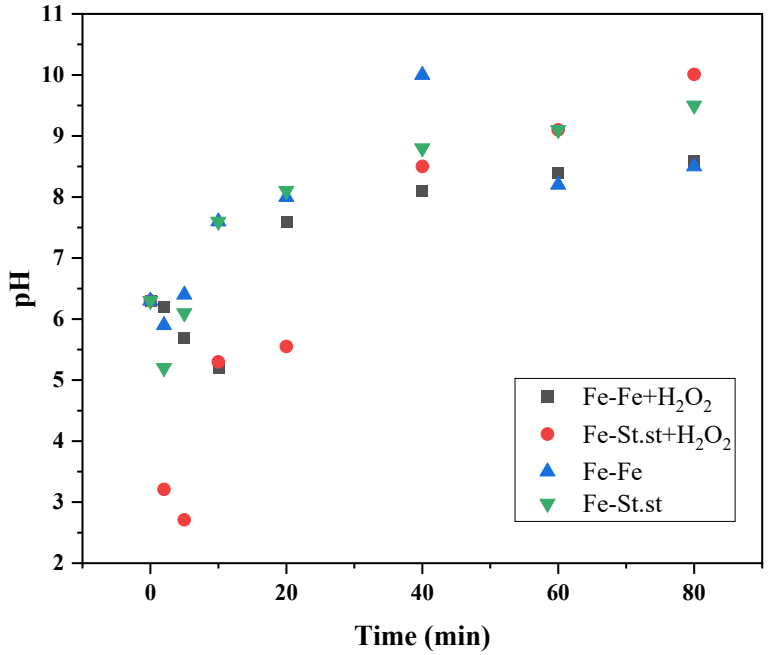

Fig. 10. The effect of pH that changes vs. time (at optimum condition, pH=6, applied current=1.2 A, and reaction time=80 min)

order reaction. Table. 10 shows the equations for all the designs.

pH variations affect

The performance of metallic electro-coagulants in their formation is influenced by the pH level of the solution, with the initial pH of the solution playing a significant role in determining their effectiveness [39, 40]. As depicted in Fig. 10, the pH value increased steadily over time. Conversely, the Cd removal efficiency continued to rise, even in the more alkaline solution. These results align with previous studies that demonstrated a significant correlation between solution pH and heavy metal removal efficiency [41]. As electricity is constantly flowing between the iron electrodes, at the cathode, hydroxyl ions are generated, whereas at the anode, Fe ions are produced, resulting in a pH gradient that affects the metals' removal efficiencies. Also, the efficiency of metal removal is affected by the production of electro-coagulants.

Estimating Thermodynamics Parameters

From Fig. 11, for the first type of electrodes, the given result is better than the second type. The positive values for ΔH indicate that the type of process is an endothermic one, the likes of which necessitate the addition of exogenous energy in the form of an electric current, as in the electrocoagulation process [42]. The positive value of ΔG signifies the nonspontaneous characteristic of the observed activity [36]. According to the findings of the researcher, the observed positive value of ΔS can be attributed to the inherent

CC BY

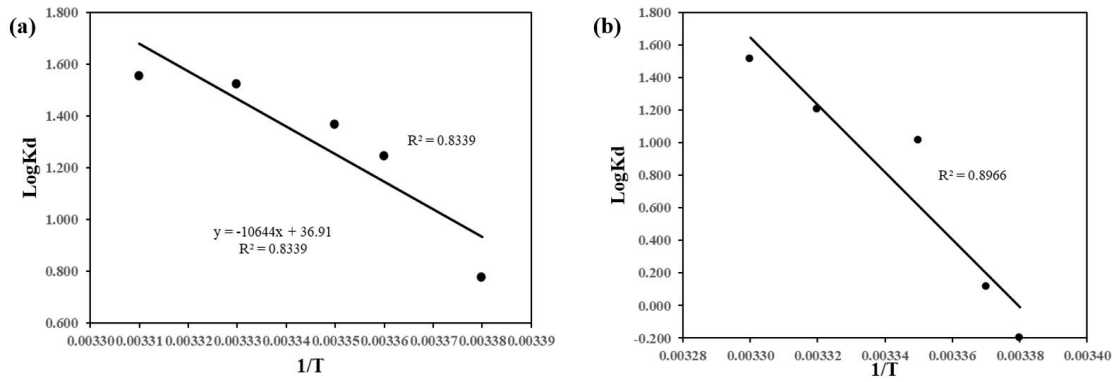

Fe-Fe presence H_2O_2 Fe-Fe absence H_2O_2

Fig. 11. The equilibrium constant (log K_d) vs. (1/T) in two different conditions with (a) and without H_2O_2 (b)

randomness and irregularity present at the interface between the liquid and solid phases [42].

The Geometry of Electrodes

The electrodes in the electrolytic cell were made from iron and stainless steel in a cylindrical shape. The active wet area for the cathode tube electrode contains holes with have diameter (2mm for each hole and with a 2cm distance between all holes, while the anode tube electrode does not contain holes. The arrangement of the electrodes in the reactor was the cathode electrode inside the anode electrode, and the wet height of the tubes of both types is the same when submerged in the contaminated solution. This new design of electrodes with the batch mode operation used gave high removal of cadmium metal with the determined parameters used from electrode material, electrode design shape, Electrolysis period, H_2O_2 concentration, pH value, Cd^{2+} concentration, and electric current. Fig. 12 shows the spectra of the components of the sludge produced for the samples treated with the two designs that suggested electrodes that were used, and found that the samples treated exhibited a considerable level of absorption within the spectral range of 400-600 cm^{-1}. The FTIR examination showed the presence of hydroxyl, carboxyl, and alkyl halides, all of which are electronegative. The presented Figure displays the FTIR spectra that show bands below 600 cm^{-1}, which have been previously shown to be indicative of metal-oxygen (M-O) vibrations in the structure of the sample. So, the vibrational modes corresponding to the peaks observed at around 470 and 540 cm^{-1} can be attributed to the Fe–O bond vibrations [43, 44]. The observed peak corresponds to the intrinsic stretching vibration of the connections formed between Cd^{2+} ions and oxygen ions [45]. Further identification of a relatively low-intensity peak within the spectral range of 480-574 cm^{-1} has been attributed to the stretching vibration of the bonds involving Fe^{3+} [46, 47]. Additionally, a distinct band seen at 488 cm^{-1} has been assigned to the stretching vibration of Fe–O bonds in Fe_3O_4, which exhibits a shift towards lower wavenumbers at 488 cm^{-1} [48]. While the M-O band appeared in the 600–550 cm^{-1}, the stretching vibration corresponding to Alkyl halides is compounds that have a C–X bond C-C_l bond appears at 555.66 cm^{-1} [49].

Practical Applications and Future Research Prospects

The results of this study present several promising avenues for practical application and future research. Optimizing the EC process using the BBD model identified optimal conditions for cadmium removal from water, reducing both experimental time and cost. Furthermore, the PEC process demonstrated its potential as a practical method, exhibiting efficient energy and electrode consumption while achieving maximum cadmium removal with cost-effective iron electrodes. The findings of this research highlight the significant potential of the PEC process for treating water and wastewater resources contaminated with heavy metals, such as cadmium.

CONCLUSIONS

This study successfully employed RSM and BBD to optimize the EC process for cadmium removal from aqueous solutions using iron electrodes. The

CC BY

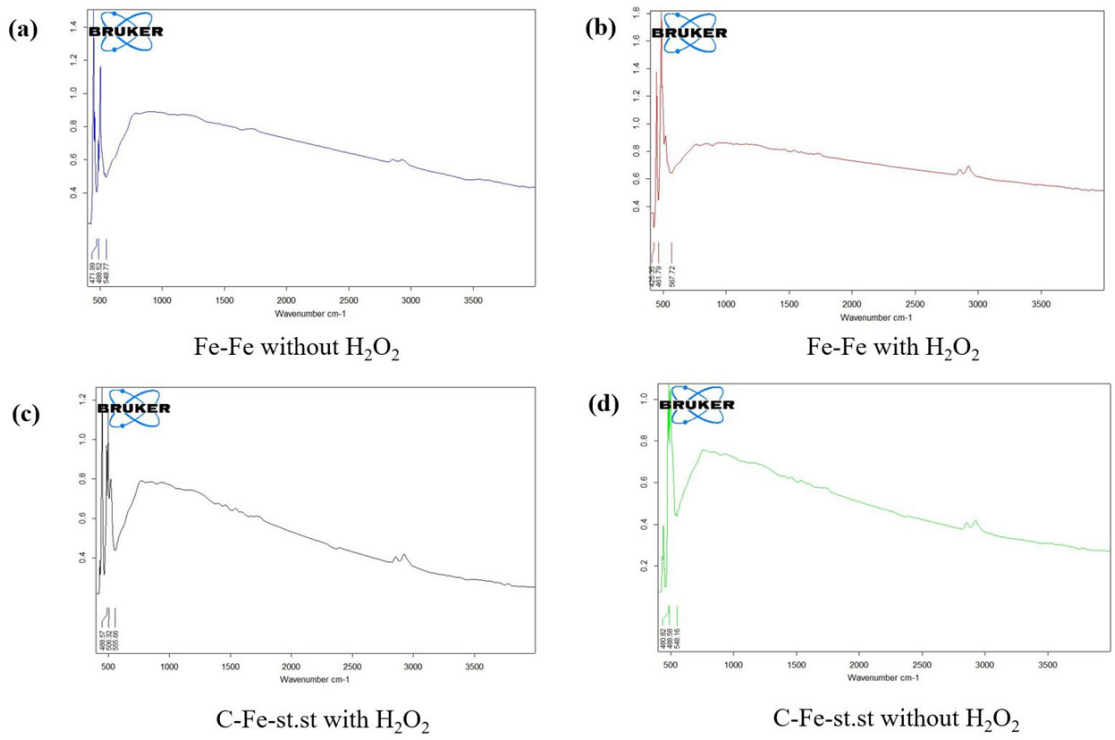

Fig. 12. FTIR spectrum for the four primary experiments

optimal EC conditions identified through BBD were subsequently applied to the PEC process. A comparative analysis was conducted to evaluate the effectiveness of PEC in the presence and absence of H_2O_2, utilizing both iron and TiO_2-coated stainless steel electrodes with non-perforated and perforated shapes. The study also investigated the influence of these variables on solution pH and temperature during the reaction. The results demonstrated the effectiveness of optimizing EC with BBD, and then using the optimum condition in the PEC process. The comparative study highlighted the impact of H_2O_2 addition and electrode material/shape on cadmium removal efficiency. Furthermore, the analysis of pH and temperature variations provided valuable insights into the reaction dynamics. Kinetic studies revealed that the metal-removal reactions followed second-order kinetics in the PEC process with the presence of H_2O_2, indicating a complex reaction mechanism. In contrast, reactions followed first-order kinetics in the PEC process without H_2O_2 and in the EC process, suggesting a simpler rate-limiting step. Thermodynamic analysis indicated that the electrocoagulation method for removing cadmium was endothermic and non-spontaneous under the studied conditions. This research contributes to a better understanding of PEC for heavy metal removal and offers a foundation for further optimization and application in real-world wastewater treatment scenarios.

CONFLICT OF INTEREST

The authors declare no conflict of interest.

REFERENCES

1. Shokri A, Mahanpoor K, Soodbar D. Degradation of 2-nitrophenol from petrochemical wastewater by UV/$NiFe_2O_4$/clinoptilolite process. 2016.
2. Doltade SB, Yadav YJ, Jadhav NL. Industrial wastewater treatment using oxidative integrated approach. S Afr J Chem Eng. 2022;40(1):100-6. https://doi.org/10.1016/j.sajce.2022.02.004
3. Benjelloun M, El Alem N, El Haddad M, El Khomsi B, El Hajjaji S. The fast-efficient adsorption process of the toxic dye onto shells powders of walnut and peanut: experiments, equilibrium, thermodynamic, and regeneration studies. Chem Afr. 2022;5(2):375-93. https://doi.org/10.1007/s42250-022-00328-1
4. Shokri A, Mahanpoor K. Using UV/ZnO process for degradation of Acid red 283 in synthetic wastewater. Bulg Chem Commun. 2018;50(1):27-32.
5. Shokri A. Photocatalytic degradation of nitrotoluene in synthetic wastewater by $CoFe_2O_4/SiO_2/TiO_2$ nanoparticles using Box-Behnken experimental design. Desalin Water Treat. 2022;247:92-9. https://doi.org/10.5004/dwt.2022.28037

CC BY

6. Yekani NH, Ghassemi A, Ghassemi M, Ghassemi M. Design and annual operation of full scale landfill leachate plant in Iran: focus on multistage membrane technology. Chem Pap. 2022;76(7):4509-21. https://doi.org/10.1007/s11696-022-02108-0
7. Shokri A, Mahanpoor K, Soodbar D. Employing UV/periodate process for degradation of p-chloronitrobenzene in aqueous environment. Desalin Water Treat. 2020;205:264-74. https://doi.org/10.5004/dwt.2020.26384
8. Njimou JR, Tchuifon DJ, Ngameni E, Nanseu-Njiki CP. Eco-friendly chitin-MnO_2-alginate nanobiocomposite spheres for enhanced heavy metal removal from wastewater. Inorg Chem Commun. 2025;172:113719. https://doi.org/10.1016/j.inoche.2024.113719
9. Shokri A. Removal of Acid red 33 from aqueous solution by Fenton and photo Fenton processes. 2017.
10. García-García A, Martínez-Miranda V, Roa-Morales G, Barrera-Díaz CE, Balderas-Hernández P. Industrial wastewater treatment by electrocoagulation-electrooxidation processes powered by solar cells. Fuel. 2015;149:46-54. https://doi.org/10.1016/j.fuel.2014.09.080
11. Fortunato GV, Oliveira MM, Silva JF, Oliveira LCA. Low Pd loadings onto Printex L6: synthesis, characterization and performance towards H_2O_2 generation for electrochemical water treatment technologies. Chemosphere. 2020;259:127523. https://doi.org/10.1016/j.chemosphere.2020.127523
12. Ren G, Zhang Y, Zhang Y, Wang Y, Wang Y. Highly energy-efficient removal of acrylonitrile by peroxi-coagulation with modified graphite felt cathode: influence factors, possible mechanism. Chem Eng J. 2018;343:467-76. https://doi.org/10.1016/j.cej.2018.02.115
13. Carneiro JF, Silva JF, Oliveira LCA, Fortunato GV. Simultaneous degradation of hexazinone and diuron using ZrO_2-nanostructured gas diffusion electrode. Chem Eng J. 2018;351:650-9. https://doi.org/10.1016/j.cej.2018.06.122
14. Alalwan HA, Alminshid AH, Alzubaidi L. A comparison study of methyl green removal by peroxi-coagulation and peroxi-electrocoagulation processes. Cleaner Eng Technol. 2023;13:100623. https://doi.org/10.1016/j.clet.2023.100623
15. Mahroudi A, Shokri A, Mahanpoor K. Removal of reactive blue 171 dye from aqueous solution and textile industrial wastewater using peroxi-electrocoagulation process by iron electrode: application of response surface methodology. Desalin Water Treat. 2022;272:266-76. https://doi.org/10.5004/dwt.2022.28821
16. Lanzalaco S, D'Antò V, Di Palma L, Petrucci E. Synthesis of polymer nanogels by electro-Fenton process: investigation of the effect of main operation parameters. Electrochim Acta. 2017;246:812-22. https://doi.org/10.1016/j.electacta.2017.06.097
17. Yao T, Zhang Y, Liu Y, Wang Y, Li J. Preparation of reduced graphene oxide nanosheet/FexOy/nitrogen-doped carbon layer aerogel as photo-Fenton catalyst with enhanced degradation activity and reusability. J Hazard Mater. 2019;362:62-71. https://doi.org/10.1016/j.jhazmat.2018.08.084
18. Xu R, Wang Y, Zhang Y, Li J, Liu Y. Removal of microplastics and attached heavy metals from secondary effluent of wastewater treatment plant using interpenetrating bipolar plate electrocoagulation. Sep Purif Technol. 2022;290:120905. https://doi.org/10.1016/j.seppur.2022.120905
19. Xia H, Zhang Y, Wang Y, Liu Y, Xu R. Simultaneous removal of organic micropollutants and inorganic heavy metals by nano-calcium peroxide induced Fenton-like treatment. Sep Purif Technol. 2023;305:122474. https://doi.org/10.1016/j.seppur.2022.122474
20. Shokri A, Nasernejad B. Electrocoagulation process for spent caustic treatment: Optimization, sludge analysis and economic studies. J Ind Eng Chem. 2024;135:471-9. https://doi.org/10.1016/j.jiec.2024.01.058
21. Eksi HS, Kazak O, Akkaya GK. Separation of oil-water emulsions by electrocoagulation and electro-persulfate with sonication pretreatment: Determination of economical electrode configuration, optimization, and comparison. Sep Purif Technol. 2024;343:127071. https://doi.org/10.1016/j.seppur.2024.127071
22. Sezer M, Yildiz Y, Aydin S, Demirbas E. Removal of microplastics in food packaging industry wastewaters with electrocoagulation process: Optimization by Box-Behnken design. Chemosphere. 2024;352:141314. https://doi.org/10.1016/j.chemosphere.2024.141314
23. Ibrahim AI, Onaizi SA, Vohra MS. Novel CTAB functionalized graphene oxide for selenium removal: adsorption results and ANN & RSM modeling. Emerg Mater. 2024;7(2):547-64. https://doi.org/10.1007/s42247-023-00570-4
24. Tak BY, Kim JH, Park JH, Yoon YH, Kim SJ. Optimization of color and COD removal from livestock wastewater by electrocoagulation process: application of Box-Behnken design (BBD). J Ind Eng Chem. 2015;28:307-15. https://doi.org/10.1016/j.jiec.2015.03.008
25. Yu Y, Zhang Y, Wang Y, Liu Y. Electrochemical behavior of aluminium anode in super-gravity field and its application in copper removal from wastewater by electrocoagulation. Chemosphere. 2021;272:129614. https://doi.org/10.1016/j.chemosphere.2021.129614
26. Horio M. Planning and Design of Multiphase Reactors. In: Tominaga H, Tamaki M, editors. Chem React React Des. 1998. p. 105-81.
27. Song J, Wang Y, Zhang Y, Liu Y, Xu R. Self-driven one-step oil removal from oil spill on water via selective-wettability steel mesh. ACS Appl Mater Interfaces. 2014;6(22):19858-65. https://doi.org/10.1021/am505254j
28. Ko YT, Lee JH, Kim SJ, Park JH. Flower-like Titanium Dioxide/Cellulose Acetate Nanofibers for Catalytic Decomposition of Organic Pollutants Including Particulate Matter Removal. Catalysts. 2024;14(4):233. https://doi.org/10.3390/catal14040233
29. Mary Rajaitha P, Rajendran S, Kumar SS, Anandan S. Graphitic carbon nitride nanoplatelets incorporated titania based type-II heterostructure and its enhanced performance in photoelectrocatalytic water splitting. SN Appl Sci. 2020;2:1-14. https://doi.org/10.1007/s42452-020-2190-9
30. Akshay V, Kumar SS, Rajendran S, Anandan S. Visible range optical absorption, Urbach energy estimation and paramagnetic response in Cr-doped TiO_2 nanocrystals derived by a sol-gel method. Phys Chem Chem Phys. 2019;21(24):12991-304. https://doi.org/10.1039/C9CP01351B
31. Kalaivani T, Anilkumar P. Role of temperature on the phase modification of TiO_2 nanoparticles synthesized by the precipitation method. Silicon. 2018;10(4):1679-86. https://doi.org/10.1007/s12633-017-9652-8
32. Liao MH, Hsu CH, Chen DH. Preparation and properties of amorphous titania-coated zinc oxide nanoparticles. J Solid State Chem. 2006;179(7):2020-6. https://doi.org/10.1016/j.jssc.2006.03.042

33. Bajpai M, Katoch SS. Reduction of COD from real graywater by electro-coagulation using Fe electrode: Optimization through box-behnken design. Mater Today Proc. 2021;43:303-7. https://doi.org/10.1016/j.matpr.2020.11.667
34. Wang JP, Chen YZ, Yuan SJ, Sheng GP, Yu HQ. Optimization of the coagulation-flocculation process for pulp mill wastewater treatment using a combination of uniform design and response surface methodology. Water Res. 2011;45(17):5633-40. https://doi.org/10.1016/j.watres.2011.08.023
35. Saleh TA, Mustaqeem M, Khaled M. Water treatment technologies in removing heavy metal ions from wastewater: A review. Environ Nanotechnol Monit Manag. 2022;17:100617. https://doi.org/10.1016/j.enmm.2021.100617
36. Abbas AM, Mohammed YI, Himdan TA. Adsorption kinetic and thermodynamic study of congo red dye on synthetic zeolite and modified synthetic zeolite. Ibn Al-Haitham J Pure Appl Sci. 2017;28(1):54-72.
37. Salman M. The equilibrium isotherm removal of chromium from wastewater by aquatic plants using batch process adsorption. Ibn Al-Haitham J Pure Appl Sci. 2009;22(3).
38. Sulaymon AH, Sharif AO, Al-Shalchi TK. Effect of tubes bundle electrode on removal of cadmium from simulated wastewaters by electrodeposition. J Chem Technol Biotechnol. 2011;86(5):651-7. https://doi.org/10.1002/jctb.2562
39. Moersidik SS, Pradana Y, Budiyono A, Sari N. Optimization and reaction kinetics on the removal of nickel and COD from wastewater from electroplating industry using electrocoagulation and advanced oxidation processes. Heliyon. 2020;6(2). https://doi.org/10.1016/j.heliyon.2020.e03319
40. Ebba M, Asaithambi P, Alemayehu E. Development of electrocoagulation process for wastewater treatment: optimization by response surface methodology. Heliyon. 2022;8(5). https://doi.org/10.1016/j.heliyon.2022.e09383
41. Bora AJ, Dutta RK. Removal of metals (Pb, Cd, Cu, Cr, Ni, and Co) from drinking water by oxidation-coagulation-absorption at optimized pH. J Water Process Eng. 2019;31:100839. https://doi.org/10.1016/j.jwpe.2019.100839
42. Richardson JF, Harker JH. Chemical Engineering - Volume 2: Particle Technology and Separation Processes. Oxford: Butterworth-Heinemann; 2002. https://doi.org/10.1016/B978-0-08-049064-9.50019-9
43. Zhang X, Zhang Y, Wang Y, Liu Y, Xu R. Effects of physical and chemical states of iron-based catalysts on formation of carbon-encapsulated iron nanoparticles from kraft lignin. Materials (Basel). 2018;11(1):139. https://doi.org/10.3390/ma11010139
44. Atta AM, Al-Lohedan HA, Al-Hussain SA. Synthesis of stabilized myrrh-capped hydrocolloidal magnetite nanoparticles. Molecules. 2014;19(8):11263-78. https://doi.org/10.3390/molecules190811263
45. Singh S, Hitkari G, Pandey G. Synthesis and characterization of cadmium doped nickel ferrite ($Ni_{0.6}Cd_{0.4}Fe_2O_4$) nanoparticles and its optical properties. Int J Sci Eng Res. 2017;8(5).
46. Chaudhari G. AC impedance spectroscopy study on nickel doped cadmium ferrites nanoparticles prepared by sol-gel citrate method. Measurements. 2014;3(10).
47. Wang T, Zhang Y, Liu Y, Xu R, Li J. Synthesis of graphene/α-Fe_2O_3 composites with excellent electromagnetic wave absorption properties. RSC Adv. 2015;5(74):60114-20. https://doi.org/10.1039/C5RA09715K
48. Dorniani D, Fakurazi S, Shaari AH, Ahmad Z, Hussein MZ. Release behavior and toxicity profiles towards leukemia (WEHI-3B) cell lines of 6-mercaptopurine-PEG-coated magnetite nanoparticles delivery system. Sci World J. 2014;2014:972501. https://doi.org/10.1155/2014/972501
49. Baharvand H. Encapsulation of ferromagnetic iron oxide particles by polyester resin. e-Polymers. 2008;8(1):102. https://doi.org/10.1515/epoly.2008.8.1.1169

CC BY